

ANNUAL REPORT

OF THE

ERWIN L. HAHN

INSTITUTE FOR

MAGNETIC

RESONANCE

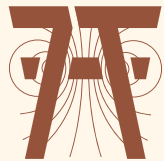
IMAGING



2015



Erwin L. Hahn Institute for Magnetic Resonance Imaging



Kokereiallee 7
D-45141 Essen
Germany

t ++49 (0)201-183-6070
f ++49 (0)201-183-6073
w www.hahn-institute.de

Preface

2015 was a very exciting year for the Erwin L. Hahn Institute given that we witnessed the insertion of the world's first 32-channel body radiofrequency (RF) coil and associated RF hardware into our centerpiece, the 7T whole-body ultrahigh field MRI system. This marks an important step after years of thorough planning, creative and courageous RF engineering and long hours of testing, all under the EU-funded 2.1 Million Euro ERC project "MRexcite" led by Mark Ladd. I have to admit that it makes me just a bit nervous to watch the 7T MRI system in the Erwin L. Hahn Institute being fragmented into its single components from time to time and then being reassembled with new components. But now all components have found their final position in the puzzle and are currently being adjusted. Our researchers have done an exceptional job managing this major task in hardware development and testing. For the years to come we hope to be able to provide 7T neuro and body MR imaging with unprecedented image quality. I invite you to share our excitement and to have a peek at the new RF body coil and at one of the world's first 7T whole-body image that you find in this annual report.

A step closer to clinical application, the EU-funded ERC grant of Tom Scheenen has enabled and supported clinically driven 7T research at the ELH in exploring the aggressiveness of prostate cancer. Tom and his group were able to show the added clinical value of 7T ultrahigh field MRI using very high spatial resolution combined with the high sensitivity achieved by 7T MRI in conjunction with a contrast agent based on ultra-small particles of iron oxide (USPIO). Using this approach, the team is now able to detect micrometastases at a very early stage. These are only two examples of the research endeavors at the ELH in the year 2015, and I invite you to take a look at further interesting research topics within this annual report.

The Institute also continues to receive marks of recognition, the highlight of which was the visit of the two Commissioners of the Province of Gelderland and Overijssel (NL), Mr. Clemens Cornielje and Mrs. Ank Bijleveld, on 13th November 2015. They were accompanied by Mr. Franz-Josef Lersch-Mense, the NRW Minister for Federal Affairs, Europe and Media. The Erwin L. Hahn Institute was recognized as an outstanding example of German-Dutch cooperation and the politicians showed great interest in the research activities at the institute.

The Erwin L. Hahn Lecture of 2015 was given by Siegfried Trattning of the Medical University of Vienna, who gave an inspiring lecture entitled 'Clinical applications at 7 Tesla: Where does it make the difference'. This was the highlight of a day-long workshop and meeting devoted to clinical applications of ultrahigh field MRI, at which Sören Johst also received the Erwin L. Hahn Award for his outstanding PhD thesis.

We look forward now to what 2016 will bring with the new 7T whole-body RF hardware being finalized and being used in first applications. We also hope that you enjoy reading this brief summary of our research activities and will continue to be interested in the activities of the Erwin L. Hahn Institute.

Harald H. Quick
Essen, February 2016



A 32-channel integrated body coil for 7 Tesla whole-body imaging

In contrast to lower field strengths, MRI systems at high field strengths of 7 Tesla and above are not equipped with an integrated body transmit coil. Due to the severe problems with B1 inhomogeneity, volume resonators are not a good choice for body applications at ultra-high fields, and local multi-channel arrays are commonly used for transmission. These arrays are often bulky and consume much of the limited space in the bore [1-3]. This restricts the patient size to those with a fairly slender body physique. By integrating a transmit array in the space between the bore liner and the gradient coil, more space would be available for the patient and further equipment like dedicated receive only coils [4]. Here we present a 32-channel transmit/receive body array integrated between the bore liner and the gradient coil.

Fig. 1A shows the array, which consists of 32 micro strip line elements with meanders arranged in 3 interleaved rings. The inner ring consists of 12 elements, while the outer rings consist of 10 elements each. The mechanical structure is made of a rigid polycarbonate frame (Fig. 1B) onto which the PCBs are glued. The front PCBs with the micro strip structure are 0.8 mm RO4003 boards with a length of 25 cm, while the ground plane is made from 0.127 mm RO4010 with 18 μ m copper plating on both sides. The ground plane is slotted to reduce eddy currents induced by the gradient coil, the slots being placed in such a way that the resulting copper strips on the front and the backside overlap. In this way, lumped capacitors only had to be used at the connection points of the end-capacitors. The overall length of the ground plane is 60 cm. The arrangement of the elements can be seen in Fig. 1C, where one half of the array is shown from the inside. The array is divided into an upper and a lower half to ease maintenance. The distance between head-on elements is 5 cm. The width of the front side PCBs is 86 mm.

All elements are connected to custom-built T/R switches [5] with an appropriate length of low-loss cable to ensure pre-amp decoupling. Detuning of the elements is performed with dedicated detuning boards containing PIN diodes that produce an RF short circuit of the transmit cable to ground when a forward current is applied.

While side-by-side neighboring micro strip lines with meanders are intrinsically well decoupled [6], they couple strongly when placed head-to-head or when they are next to each other but shifted in the longitudinal direction. Thus, decoupling networks were used to decrease coupling between some of the neighboring elements. There are 50 of these networks for the complete array. There are no decoupling networks connecting the two halves of the array, where the adjoining elements are side-by-side.

To enable usage of the 32ch array together with local receive coils, a custom built PIN-diode controller was used to provide forward current and reverse voltage for the PIN diodes, and the receive chain of the MRI system was extended with 32ch switches and a 32ch 2nd-stage receive amplifier with bias tees for power supply of the pre-amps [7].

A custom-built 32ch pTx system including custom RF amplifiers and RF modulators was used to drive the array during transmit.

The highest coupling between elements occurs where the two halves of the array connect. Here the coupling is -14 dB when loaded with a volunteer centered on the abdominal region.

Overall noise correlation is low; the maximum value is 22%. This value occurs between the elements that border the array halves.

Table 1 shows the in vivo g-factors in an axial slice through the abdomen of a male volunteer (1.72m, 65kg), showing the means as well as maximums.

Fig. 2 shows the first in vivo dataset. The entire body is covered in 4 stations. The images appear fairly homogeneous over a 500mm field-of-view. TIAMO was used for homogenization. The g-factors are quite high for an array with 32 channels. The reason for this is most probably the large distance between the array elements and the body, leading to high correlations between the sensitivities of the elements. To enhance the receive performance, a dedicated receive array could be used, which is feasible since the changes in the receive chain allow for computer-controlled switching between reception with the body array or a local receive array.

First tests with the presented 32ch array show promising results. The entire body of a human volunteer could be covered quite uniformly in only 4 stations.

Acknowledgments

The research leading to these results has received funding from the European Research Council under the European Union's Seventh Framework Programme (FP/2007-2013) / ERC Grant Agreement n. 291903 MRXcite.

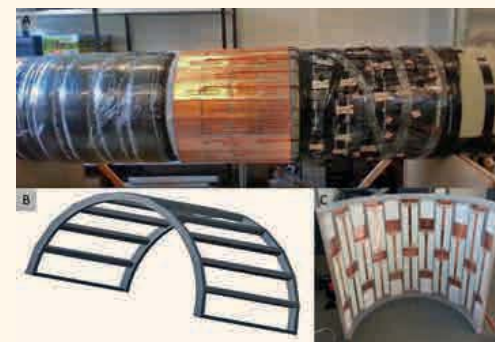


Fig.1: A) The body array on the bore liner. On the right, the T/R switches and detuning boards are visible; B) CAD model of one half of the polycarbonate frame used to hold the PCBs; C) Inner surface of one half of the polycarbonate frame with the PCBs glued on.

		g-factor LR				
		R=2	R=3	R=4	R=6	R=8
g-factor AP	R=1	1.02/1.25	1.08/2.21	1.30/3.72	1.63/4.85	2.17/9.57
	R=2	1.06/1.32	1.17/2.04	1.62/4.37		
	R=3	1.14/2.51	1.30/3.06	1.70/7.2		
	R=4		1.62/4.32	2.21/10.61		

Table 1: g-factors (mean/max) in AP and LR directions in a central abdominal slice when the array is loaded with a male volunteer.



Fig. 2: First in vivo dataset of a male volunteer of 1.72 m and 65 kg acquired with a 2D FLASH sequence. The entire body was covered in 4 stations, each with a 500 mm by 500 mm field-of-view with a 10 cm overlap. The echo time was 6.2 ms, the resolution is 1.95 x 1.95 x 5 mm³.

References

- [1] Metzger GJ, van de Moortele PF, Akgun C, Snyder CJ, Moeller S, Strupp J, Andersen P, Shrivastava D, Vaughan T, Ugurbil K, Adriany G (2010). Performance of external and internal coil configurations for prostate investigations at 7 T. *Magn Reson Med* 64 (6):1625-1639.
- [2] Orzada S, Quick HH, Ladd ME, Bahr A, Bolz T, Yazdanbakhsh P, Solbach K, Bitz AK (2009). A flexible 8-channel transmit/receive body coil for 7 T human imaging. In: Proceedings of the 17th scientific meeting, International Society for Magnetic Resonance in Medicine, Honolulu, p 2999.
- [3] Raaijmakers AJ, Ipek O, Klomp DW, Possanzini C, Harvey PR, Lagendijk JJ, van den Berg CA (2011). Design of a radiative surface coil array element at 7 T: the single-side adapted dipole antenna. *Magn Reson Med* 66 (5):1488-1497.
- [4] Vaughan JT, Snyder C, Delabarre L, Tian J, Adriany G, Andersen P, Strupp J, Ugurbil K (2009). Clinical Imaging at 7T with a 16 Channel Whole Body Coil and 32 Receive Channels. In: Proceedings of the 17th scientific meeting, International Society for Magnetic Resonance in Medicine, Honolulu, p 392.
- [5] Watkins RD, Caverly RH, Doherty WE (2012). 298MHz Micro miniature 2KW Transmit Receive Switch for 7.0 Tesla TR Arrays. *Proc Intl Soc Mag Reson Med* 20:2686.
- [6] Rietsch SHG, Quick HH, Orzada S (2015). Impact of different meander sizes on the RF transmit performance and coupling of microstrip line elements at 7 T. *Med Phys* 42 (8).
- [7] Orzada S, Bitz AK, Solbach K, Ladd ME (2015). A receive chain add-on for implementation of a 32-channel integrated Tx/Rx body coil and use of local receive arrays at 7 Tesla. In: Proceedings of the 23rd scientific meeting, International Society for Magnetic Resonance in Medicine, Toronto, p 3134.

Changes in glutamate and GABA measured with proton magnetic resonance spectroscopy of the brain

Jan-Willem Thielen, Seyedmorteza Rohani Rankouhi, Donghyun Hong, Indira Tendolkar, David G. Norris

Introduction

The Helmholtz Alliance ICEMED is a network of complementary research excellence representing a worldwide unique research consortium of biomedical research scientists, clinicians and cutting edge metabolic imaging experts in Germany. ICEMED consists of more than 30 leading German diabetes and obesity research teams and research centres. The alliance will focus on identifying, visualizing, dissecting and targeting neural pathways (in both central control circuits and brain-periphery crosstalk) that regulate systems metabolism. This aspect of the alliance is synergistically enhanced by the integration of comprehensive neuroimaging expertise. The role of the Erwin L Hahn Institute in this project is to investigate whether aerobic exercise improves cognitive performance in type 2 diabetes (T2DM) using GABA and glutamate/glutamine, (GLX) spectroscopy (MRS) and MRI at 7 Tesla. To achieve this goal we have established two parallel and converging lines of research (neuroscientific and MRS techniques).

In the neuroscientific line we examined connectivity and metabolic changes during memory formation. MRS was performed before and after a face-name association task in the scanner (MRS1, MRS2). Performance was subsequently measured (outside the scanner, Fig. 3A).

The MRS analysis (3B) showed that GLX but not GABA concentrations changed over time due to the memory task. The upper right panel (3B) shows that the increase in GLX over time correlates positively with the GABA concentration. Thus, subjects with higher levels of medial prefrontal cortex (mPFC) GABA concentrations showed a greater increase in GLX concentrations. The left panel at the bottom of (3B) shows that memory performance correlates positively with GABA concentration. The right panel shows that the change in GLX concentration (GLX MRS 2 minus GLX MRS 1) correlates positively with memory performance. Fig. 3C shows the outcome of the fMRI analysis. The black dotted square indicates the position of the MRS voxel. We found task related brain activation in the mPFC (yellow cluster in the MRS voxel). This cluster was functionally connected to the thalamus (white arrow) during the encoding of items that were

confidently remembered. The middle panel shows that the functional connectivity correlates positively with memory performance and the right panel that it correlates with the change in GLX concentration. Taken together, we show that the formation of new episodic memories is associated with GABA/ GLX concentrations in the mPFC. We found that brain processes inherent to memory formation cause an increase in GLX concentration which is related to the amount of GABA. Moreover, this effect appears to be related to functional connectivity between mPFC and thalamus and performance on the face-name association task.

The developments in the MRS techniques line aim to maximise the sensitivity of GABA spectroscopy and to ameliorate the effects of inhomogeneities of both the static and radiofrequency magnetic fields. For example, we have looked at optimising the signal combinations from phased array coils, based on the SNR of GABA. This technique made it possible to increase the sensitivity for deeper voxels, like the thalamus by 20% compared to the standard method. We have also implemented the MEGA-sLASER techniques as an efficient MRS method to measure GABA in human brain at 7T. This provides good localization with minimal chemical shift artifacts and insensitivity to variations in the radiofrequency field through the use of adiabatic RF pulses. GABA editing was achieved with a pair of dual band narrow bandwidth inversion pulses. Single voxel MRS data were collected from 20x20x20 mm³ voxels positioned at anterior cingulate (AC), motor cortex (MC) and occipital cortex (OC) (TR=4500 ms, TE=80 ms, averages=64, scan time=5:06 mins). Example spectra from one subject obtained from the three regions are shown below. GABA+ and Glx are seen at 3 ppm and 3.75 ppm respectively.

Perspective

We are currently working on combining the methods developed with a study of the benefits of exercise on diabetic patients. This is a long term study performed in collaboration with the German diabetes centre in Düsseldorf.

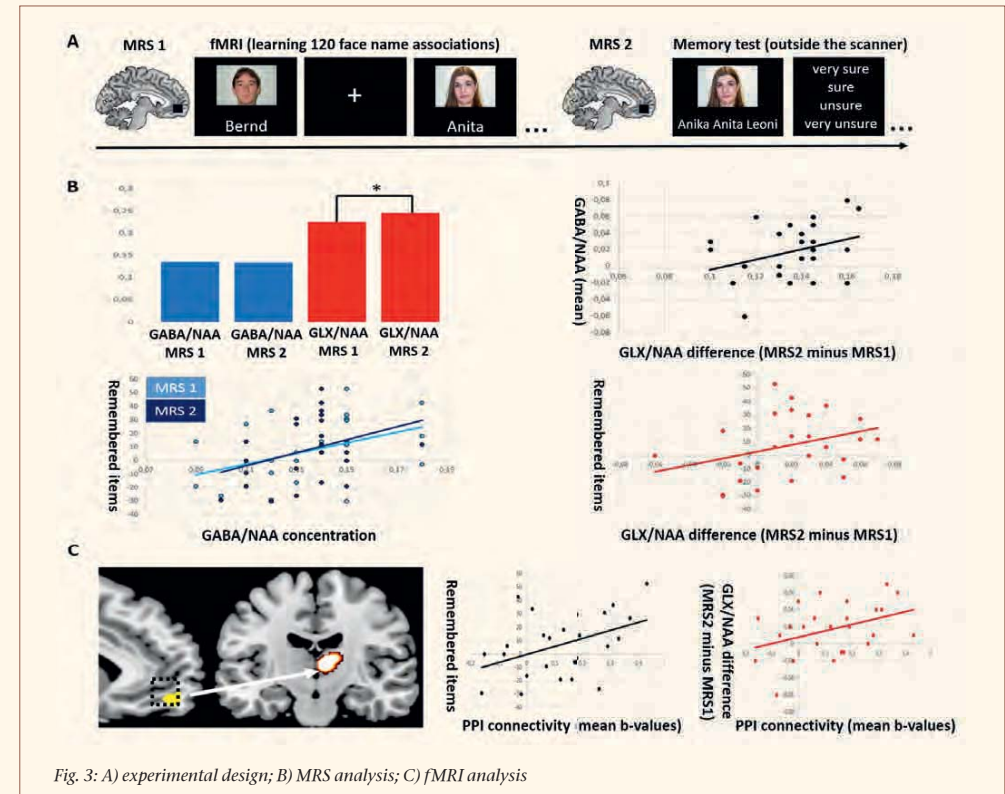


Fig. 3: A) experimental design; B) MRS analysis; C) fMRI analysis

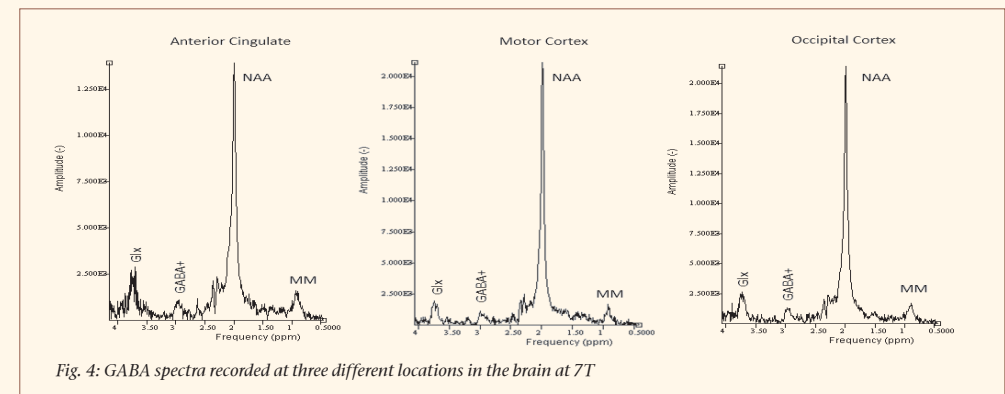


Fig. 4: GABA spectra recorded at three different locations in the brain at 7T

Radiofrequency Coils and Signal Homogenization in 7T UHF MRI

Towards new clinical applications of 7T UHF MRI

Harald H. Quick

The research group High Field and Hybrid MR Imaging directed by Professor Harald H. Quick in the year 2015 continued to develop and evaluate new techniques and methods to broaden the spectrum of clinical applications of 7-Tesla ultrahigh-field magnetic resonance imaging (7T UHF MRI). Specifically, new multi-channel radiofrequency (RF) transmit/receive coils for 7T neuro and body MR imaging are simulated, designed, and evaluated [1,2]. The ultimate aim is to assess the high signal-to-noise-ratio (SNR) inherent to UHF-MRI and to apply this to high resolution imaging in various diagnostic applications (Fig. 5 and 6). The research groups of Prof. Harald Quick and Prof. Mark Ladd (DKFZ, Heidelberg) work in close cooperation to achieve this aim. Further active collaborations in the field of RF coil development exist with technical development partners in RF Technology Engineering (Prof. Klaus Solbach) and Electrical Engineering (Prof. Daniel Erni) of the University of Duisburg-Essen. Numerous collaborations with clinical users of 7T UHF MRI from the University Hospital Essen have been established to advance clinical applications at

7T field strength. Here, the Department of Radiology (Prof. Michael Forsting and Dr. Lale Umutlu) and the Department of Neurosurgery (Prof. Ulrich Sure and Dr. Karsten Wrede) are to be mentioned to cover 7T clinical research applications from head to whole-body imaging [3-8]. Field strength comparison studies serve to evaluate the potential advantages and disadvantages of 7T UHF MRI when compared to the clinical standard field strengths 1.5T and 3T MRI. A further research focus is on safety aspects when imaging patients with passive and active implants. As in previous years, the instrument of intramural funding of the Medical Faculty of the University of Duisburg-Essen (IFORES Program) also in the year 2015 was successfully acquired to support clinical researchers from Radiology and Pediatrics conducting their 7T MRI projects during a 12-months research period at the ELH Institute.

Current research topics of the research group High Field and Hybrid MR Imaging in 7-Tesla ultrahigh-field MRI are the following.

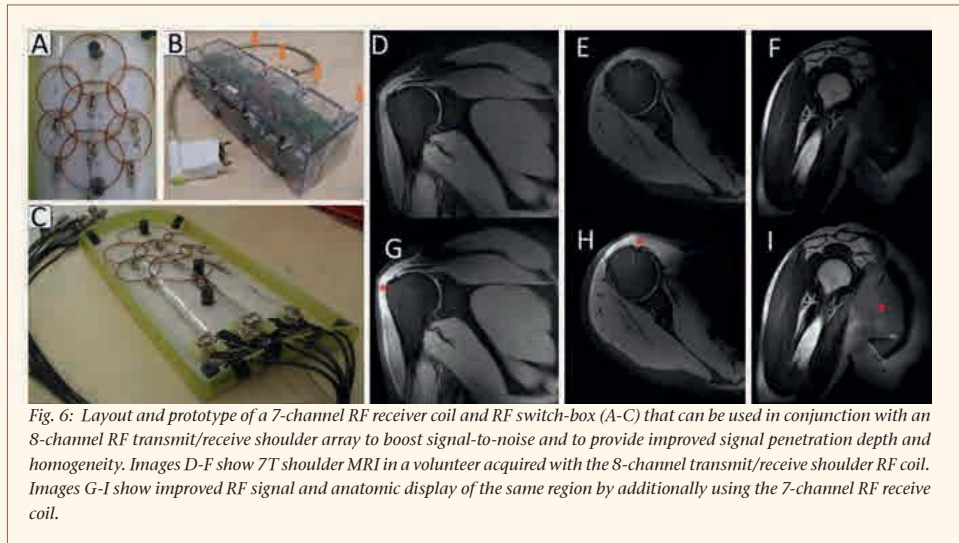


Fig. 6: Layout and prototype of a 7-channel RF receiver coil and RF switch-box (A-C) that can be used in conjunction with an 8-channel RF transmit/receive shoulder array to boost signal-to-noise and to provide improved signal penetration depth and homogeneity. Images D-F show 7T shoulder MRI in a volunteer acquired with the 8-channel transmit/receive shoulder RF coil. Images G-I show improved RF signal and anatomic display of the same region by additionally using the 7-channel RF receive coil.

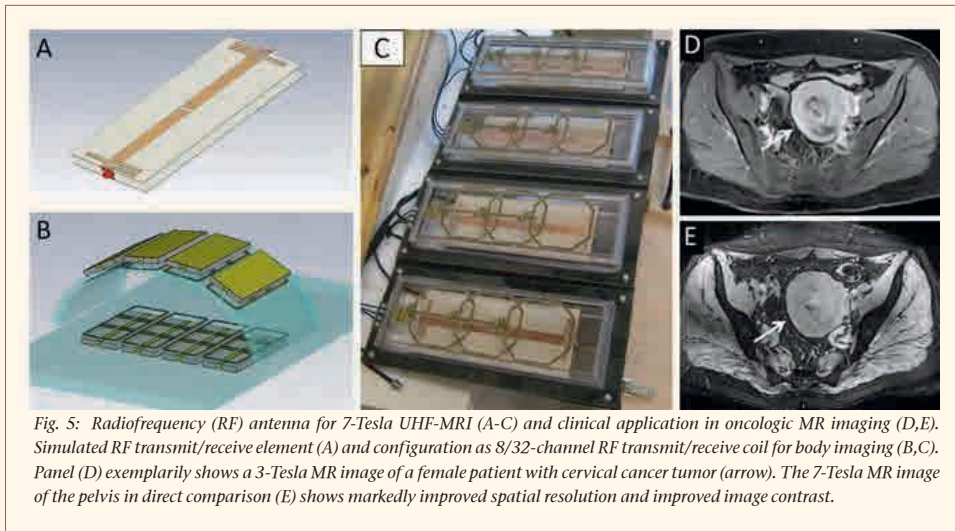


Fig. 5: Radiofrequency (RF) antenna for 7-Tesla UHF-MRI (A-C) and clinical application in oncologic MR imaging (D,E). Simulated RF transmit/receive element (A) and configuration as 8/32-channel RF transmit/receive coil for body imaging (B,C). Panel (D) exemplarily shows a 3-Tesla MR image of a female patient with cervical cancer tumor (arrow). The 7-Tesla MR image of the pelvis in direct comparison (E) shows markedly improved spatial resolution and improved image contrast.

Development, evaluation, and clinical application of:

- multichannel radiofrequency (RF) transmit/receive coils and RF components
- concepts for B1 signal homogenization
- methods and techniques for 7-Tesla UHF-MRI
- applications for 7-Tesla UHF-MRI in body and cardiovascular imaging
- clinical comparison studies between 1.5-, 3- and 7-Tesla UHF-MRI
- safety concepts for UHF-MRI of passive and active implants

- [5] Matsushige T, Chen B, Dammann P, Johst S, Quick HH, Ladd ME, Forsting M, Sure U, Wrede KH (2015). Microanatomy of the subcallosal artery: an in-vivo 7 T magnetic resonance angiography study. *Eur Radiol.* [Epub ahead of print]
- [6] Lazik A, Theysohn JM, Geis C, Johst S, Ladd ME, Quick HH, Kraff O (2015). 7 Tesla quantitative hip MRI: T1, T2 and T2* mapping of hip cartilage in healthy volunteers. *Eur Radiol.* [Epub ahead of print]
- [7] Hahnemann ML, Kraff O, Orzada S, Umutlu L, Kinner S, Ladd ME, Quick HH, Lauenstein TC (2015). T1-Weighted Contrast-Enhanced Magnetic Resonance Imaging of the Small Bowel: Comparison Between 1.5 and 7 T. *Invest Radiol.* 50(8):539-47. doi: 10.1097/RLI.0000000000000161.
- [8] Hahnemann ML, Kraff O, Maderwald S, Johst S, Orzada S, Umutlu L, Ladd ME, Quick HH, Lauenstein TC (2015). Non-enhanced magnetic resonance imaging of the small bowel at 7 Tesla in comparison to 1.5 Tesla: first steps towards clinical application. *Magn Reson Imaging.* pii: S0730-725X(15)00344-6. doi: 10.1016/j.mri.2015.11.012. [Epub ahead of print]

References

- [1] Rietsch SH, Quick HH, Orzada S. Impact of different meander sizes on the RF transmit performance and coupling of microstrip line elements at 7 T (2015). *Med Phys.* 42(8):4542-52. doi: 10.1118/1.4923177.
- [2] Remmings A, Solbach K, Quick HH. Evaluation of electronic band gap (EBG) radiofrequency (RF) coil concepts for MRI. *DFG 154-3-2*, 2016-2017.
- [3] Moenninghoff C, Kraff O, Maderwald S, Umutlu L, Theysohn JM, Ringelstein A, Wrede KH, Deuschl C, Altmepfen J, Ladd ME, Forsting M, Quick HH, Schlamann M. Diffuse axonal injury at ultra-high field MRI (2015). *PLoS One* 10(3):e0122329. doi: 10.1371/journal.pone.0122329. eCollection 2015.
- [4] Matsushige T, Chen B, Ringelstein A, Umutlu L, Forsting M, Quick HH, Sure U, Wrede KH (2015). Giant Intracranial Aneurysms at 7T MRI. *AJNR Am J Neuroradiol.* [Epub ahead of print]

How do people perceive robots and are they really uncanny?

Uncanny valley related behavioral responses are driven by neural processes of face perception

The uncanny valley hypothesis states that the more humanlike robots become the greater people feel familiar with these robots or perceive these robots as more likable, respectively, and are more willing to accept them (Mori, 1970). However, shortly before the ideal of perfect humanness the curve breaks in and familiarity reverses into uncanniness. Proposed explanations for the uncanny valley effect can be classified as perception-oriented approaches, evolutionary-biological approaches, and cognitive-oriented approaches.

The underlying assumption for the perception-oriented approaches explanations is a mismatch between expectations about perceptions and actual

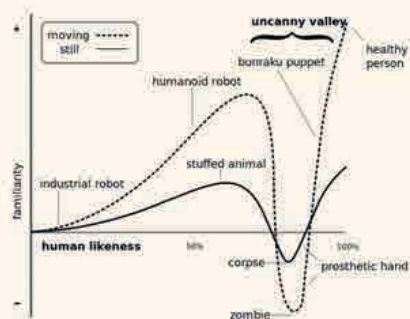


Fig. 7: The graph depicts the uncanny valley, the proposed relation between the human likeness of an entity and the perceiver's affinity for it. Figure by Smurrayinchester [CC-BY-SA-3.0 (<http://creativecommons.org/licenses/by-sa/3.0/>)], via Wikimedia Commons

perceptions in whatever form, which causes some kind of additional processing on how to interpret, categorize, or react to this phenomenon. It has been assumed that this state of additional processing elicits some kind of uncertainty or cognitive dissonance which is subsequently negatively interpreted and thus the origin of the uncanny valley effect [1].

As another possible explanation it has been proposed that uncanny valley responses might be due to an evolutionary developed mechanism to avoid the risk of infection and the risk of genetically inadequate

mating partners [2] which is disgust. Although, not only people, but also objects possess particular types of prepared features that connote disease [5] (and hence elicit disgust reactions), it is expected that the likability for such a reaction increases with increased human-likeness, because then the object will be more likely classified as conspecific [4] and "if a feature on a conspecific stimulus is sufficiently atypical, then it can be expected to trigger one of these mechanisms independently of any real danger" (p. 760).

We systematically tested perception-oriented and evolutionary-biological explanatory approaches for the uncanny valley. More specifically, we examined whether uncanny valley related reactions are observable in participants' evaluations of humans and robots with regard to uncanny valley related rating dimensions (likability, familiarity, human-likeness) and regarding behavioral measures (decision making, cf. Fig. 9). Subsequently, it was analyzed whether these behavioral effects, if detectable, can be explained by the proposed explanations. For this purpose, relations between behavioral measures and activity in relevant brain areas will be analyzed. In contrast to previous work the set of stimulus material did not only include different groups of robots (mechanoid, humanoid, android), but also different groups of humans (healthy humans, disabled humans, "artificial" humans, cf. Fig. 7) in order to reflect the far right end of the graph depicted by Mori and address the fact that also human stimuli can vary in human-likeness. Participants (n=26, 14 female, all right handed; aged between 18 and 35 years (M = 23.04, SD = 4.47)) had to rate six categories of stimuli: healthy humans, disabled humans, artificial humans, android robots, humanoid robots and mechanoid robots. During the decision trials participants had to choose one of two presented stimuli with regard to the question from whom they would like to receive a reward (under the condition that several rewards can be given, every presented human or robot has chosen a reward prior to the experiment and this choice is unknown to the participants).

Considering all results from the self-report measures, behavioral data and neuroimaging data there are several important implications for the

Astrid Rosenthal-von der Pütten, Fabian Grabenhorst
Matthias Brand, Nicole Krämer



Fig. 8: Examples of stimuli

uncanny valley hypothesis. Evaluations of humans and robot are indeed driven by perception of human-likeness as indicated by the results of the regression analyses. Furthermore, evaluations of human-likeness strongly depend on the neural processes of face perception. Thus, "smooth" face processing of actual human faces leads to higher ratings of human-likeness and consequently to more positive ratings on other dimensions. In contrast, additional processing caused by incompatible template-activators (robot faces) or flawed human faces is connected to lower ratings in human-likeness and thus a more negative evaluation on other dimensions. However, flawed faces and incompatible template activators caused increased activity in different areas of the fusiform gyrus, although behavioral effects were similar. Human-likeness elicits mentalizing or theory of mind processes. Hence, more human-like stimuli such as healthy, disabled and artificial humans as well as android robots elicited activation in theory of mind associated brain areas. In general, it was observable that participants decided in favor for those stimuli which caused increased

activity in the related areas. Altogether, the current work significantly contributed in defining what effect human-likeness has with regard to uncanny valley related reactions on a neural, self-report and behavioral level and how these reactions relate to each other. Moreover, the present study found strong support for perception-oriented explanations for the uncanny valley effect. First, effects seem to be driven by the aforementioned phenomena in face perception. Further there were indicators for the assumption that categorical perception takes place. However, since the experimental paradigm was not explicitly designed to test for categorical perceptions the conclusions here are preliminary and need further investigation. In the contrary, evolutionary-biological driven explanations assuming that uncanny valley related reactions are due to oversensitivity of the behavioral immune system were not supported by this work.

References

- [1] MacDorman KF, Green RD, Ho CC, Koch CT (2009). Too real for comfort: Uncanny responses to computer generated faces. *Computers in Human Behavior* 25, 695–710.
- [2] MacDorman KF, Ishiguro H (2006). The Uncanny Advantage of Using Androids in Cognitive and Social Science Research. *Interaction Studies* 7, 3, 297–337.
- [3] Mori M (1970). The uncanny valley. *Energy* 7, 4, 33–35.
- [4] Burleigh TJ, Schoenherr JR, Lacroix GL (2013). Does the uncanny valley exist? An empirical test of the relationship between eeriness and the human likeness of digitally created faces. *Computers in Human Behavior* 29, 3, 759–771.
- [5] Oaten M, Stevenson RJ, Case TI (2009). Disgust as a disease-avoidance mechanism. *Psychological Bulletin* 135, 2, 303–321.

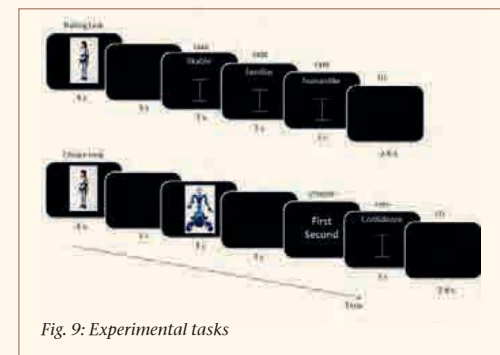


Fig. 9: Experimental tasks

Multi-parametric MR imaging of the prostate at 7T

Feasibility of high-resolution T2-weighted imaging, diffusion weighted imaging and 1H MR spectroscopic imaging of the prostate at 7T

Multiparametric magnetic resonance imaging (mpMRI) has been shown to be effective for the detection, localization and local staging of prostate cancer [1-4] and in guiding prostate biopsies in men with previous negative findings [5]. An mpMRI prostate protocol consists of high-resolution T2-weighted (T2W) MR imaging and at least two functional MR techniques: diffusion-weighted imaging (DWI), dynamic contrast-enhanced (DCE) MRI and/or proton MR spectroscopic imaging (1H MRSI).

In clinical practice magnetic field strengths of 1.5 and 3T are used for mpMRI, sometimes with an endorectal coil for MR signal detection. Ultra-high field-strength (7T and higher) MR systems offer an increased signal-to-noise ratio (SNR), theoretically enabling improvements in spatial resolution of the SNR-limited mpMRI techniques: T2W-MRI, DWI and 1H MRSI. In addition, the high SNR facilitates the study of new biomarkers for prostate cancer using 31P MRSI [6]. The combination of an external transmit array coil with an endorectal receive coil increases local sensitivity and allows for reduced fields of view, enabling higher resolution prostate images [7]. This coil combination also creates opportunities for DWI and fast 1H MRSI, with pulse sequences dedicated to overcome the 7T related technical challenges.

In this study we assessed the technical feasibility of mpMRI of the prostate at 7T including T2W-MRI, DWI and 1H MRSI using the combination of an external 8-channel transmit array coil and an endorectal receive coil.

Fourteen patients with biopsy-proven prostate cancer (mean age: 65.2 years; median PSA level: 6.2 ng/mL; median Gleason score: 6) were recruited for this study, after they had undergone a clinical 3T mpMRI examination of the prostate. The full MRI protocol at 7T included triplanar T2W turbo spin-echo imaging, DWI and 3D 1H-MRSI. Sequence optimization for T2W-MRI was presented previously [6], the receive only endorectal coil allowed for an increase in spatial resolution ($0.3 \times 0.3 \times 2.0 \text{ mm}^3$, TE 85 ms). The number of slices was adjusted to cover the full prostate

(12-25 slices). DWI was performed using a 5-shot readout segmented echo-planar imaging sequence, including a 2D navigator echo to correct for non-linear phase-errors [7], with b-values of 0, 100, 400 and 800 s/mm^2 ($1.75 \times 1.75 \times 2.0 \text{ mm}^3$, TE 68 ms). Metabolite levels within the prostate were measured using a dedicated 3D 1H-MRSI sequence using spectral-spatial pulses for volume selection [8] (0.5 to 0.9 cm^3 spherical voxels). Two radiologists in consensus performed a qualitative comparison of the images to 3T.

In a typical example of a patient with low-Gleason cancer the lesion appears as a hypo intense area in the T2W images and as a focus of restricted diffusion on the ADC maps (Fig. 10). The 7T diffusion-weighted b-value images show a strong T2-weighting, masking the effect of the tumor on the diffusion. The tumor spectrum shows relative low citrate levels with respect to spermine levels, choline could not be identified because of the large linewidth of spermine. In this example the overall image quality of the 7T transversal T2W images and DWI was rated fair and good, respectively. Structure delineation and contrast of the T2W image series as well as the quality of the DWI was judged similar to 3T.

Overall T2W image and DWI quality at 7T was scored as fair (3/5, 38% and 17% respectively) to good or very good (4/5 and 5/5, 55% and 83% respectively). 24% of the T2W image series showed an improvement in structure delineation compared with 3T. MRSI quality was rated fair or good in 56% of the acquisitions.

In conclusion, multiparametric MRI of the prostate at 7T is feasible at unprecedented spatial resolutions for T2W-imaging and DWI and within clinically acceptable acquisition times for high resolution 1H-MRSI. The higher spatial resolutions can yield better delineation of prostate anatomy, but the robustness of the techniques needs to be improved before clinical adoption of 7T mpMRI.

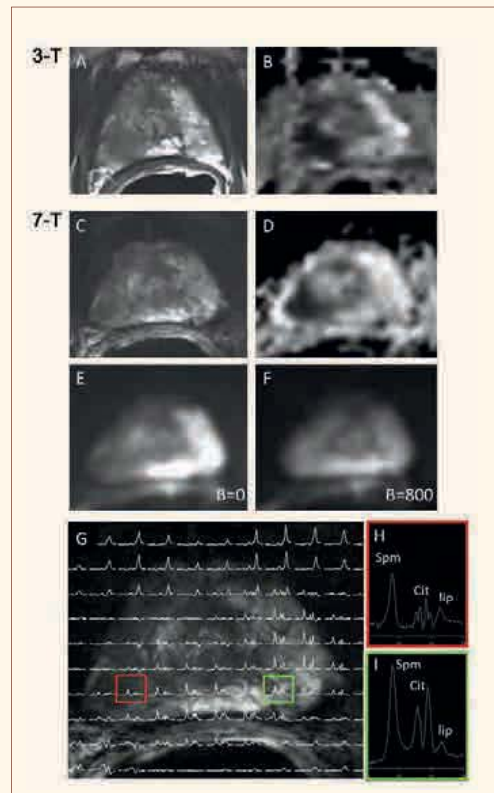


Fig. 10: mpMRI of a prostate tumor in a 65-year old patient. A significant lesion is visible both in the 3T (A,B) and 7T images (D-I). A,C: T2W-MRI; B,D: ADC map; E,F: diffusion weighted images with $b = 0 \text{ s/mm}^2$ (E) and $b = 800 \text{ s/mm}^2$ (F); G: spectral map of 1H-MRSI; H: spectrum of lesion, I: spectrum of normal-appearing contralateral peripheral zone tissue. Cit: citrate; lip: lipids; Spm: spermine.

References

- [1] Kim JY, Kim SH, Kim YH, Lee HJ, Kim MJ, Choi MS (2014). Low-Risk Prostate Cancer: The Accuracy of Multiparametric MR Imaging for Detection. *Radiology*; 271: 435-444.
- [2] Johnson LM, Turkbey B, Figg WD, Choyke PL (2014). Multiparametric MRI in prostate cancer management. *Nat. Rev. Clin. Oncol.* 11: 346-353.
- [3] de Rooij M, Hamoen EHJ, Fütterer JJ, Barentsz JO, Rovers MM (2014). Accuracy of multiparametric MRI for prostate cancer detection: a meta-analysis. *AJR Am. J. Roentgenol.* 202: 343-351.
- [4] Scheenen TWJ, Rosenkrantz AB, Haider MA, Fütterer JJ (2015). Multiparametric Magnetic Resonance Imaging in Prostate Cancer Management: Current Status and Future Perspectives. *Invest. Radiol.*; doi:10.1097/RLL.0000000000000163.
- [5] Farnell T, Stephan C, Erbersdobler A, Dietz E, Maxeiner A, Hell N, Huppertz A, Miller K, Strecker R, Hamm B. (2011). Areas suspicious for prostate cancer: MR-guided biopsy in patients with at least one transectal US-guided biopsy with a negative finding—multiparametric MR imaging for detection and biopsy planning. *Radiology* 259: 162-172.
- [6] Maas MC, Vos EK, Lagemaat MW, Bitz AK, Orzada S, Kobus T, Kraff O, Maderwald S, Ladd ME, Scheenen TWJ (2014). Feasibility of T2-weighted turbo spin echo imaging of the human prostate at 7 tesla. *Magn. Reson. Med.* 71: 1711-1719.
- [7] Porter DA, Heidemann RM (2009). High resolution diffusion-weighted imaging using readout-segmented echo-planar imaging, parallel imaging and a two-dimensional navigator-based reacquisition. *Magn. Reson. Med.* 62: 468-475.
- [8] Lagemaat MW, Breukels V, Vos EK, Kerr AB, van Uden MJ, Orzada S, Bitz AK, Maas MC, Scheenen TWJ (2015). 1H MR spectroscopic imaging of the prostate at 7T using spectral-spatial pulses. *Magn. Reson. Med.*; doi:10.1002/mrm.25569.

In vivo assessment of the cerebellum by novel MRI techniques and application to hereditary ataxias

Morphological, pathoanatomical and clinical aspects

Degenerative ataxias are slowly progressive disorders which affect the cerebellum and cerebellar pathways to various degrees. Both hereditary and nonhereditary forms of degenerative ataxia fall under the category of rare neurological diseases. Key symptoms are motor incoordination and disordered balance, manifesting themselves in limb ataxia, ataxia of stance and gait, dysarthria, and oculomotor signs.

There are three well-known types of macroscopic damage associated with degenerative ataxias which can be readily observed in diagnostic brain scans: cortical cerebellar atrophy, olivopontocerebellar atrophy, and spinal atrophy [3]. As yet, assessment of the deep cerebellar nuclei is not part of the diagnostic routine. The iron content in the cerebellar nuclei is high, and susceptibility weighted imaging (SWI) allows visualization of the cerebellar nuclei and quantification of their volume in healthy subjects [4,5]. Histological data reveal that the iron-rich deep cerebellar nuclei are pathologically affected to various extents, resulting in atrophy and altered iron metabolism in degenerative ataxias. Preliminary work by Dagmar Timmann and Mark Ladd, which was funded by a Marie Curie Initial Training Network (ITN), suggests that SWI is helpful to diagnose and quantify accompanying atrophy of the cerebellar nuclei in hereditary ataxias [6,7].

The study by Stefanescu et al. (2015) included patients with three types of hereditary ataxias: Friedreich's ataxia (FRDA), which is the most common recessive ataxia in Europe and the USA, and spinocerebellar ataxias type 3 and 6 (SCA3, SCA6), which are among the most common autosomal dominant ataxias. Whereas marked cerebellar atrophy and reduction of gray matter volume is a hallmark of SCA6, cerebellar atrophy is uncommon in FRDA and comparatively mild in SCA3, at least in the early stages of the disease (Fig. 11, top row). Atrophy of the spinal cord is a characteristic finding in Friedreich's ataxia. Cerebellar nuclei have long been thought to be preserved in SCA6, whereas histology shows marked atrophy of the nuclei in FRDA and SCA3. The hypothesis was tested that cerebellar nuclei are smaller in FRDA and SCA3 compared to healthy controls, but relatively preserved in SCA6. SWI allowed depiction of atrophy of the cerebellar nuclei in patients with FRDA and SCA3. In SCA6, pathology was not restricted to the cerebellar cortex but also involved the cerebellar nuclei, confirming more recent histological findings. In fact, volume reduction of the nuclei was most marked in SCA6 (Fig. 11, bottom row).

SWI, however, faces several limitations that include its non-quantitative nature and the inherent blooming effect of iron deposits on the images. Thus, the extent of the cerebellar

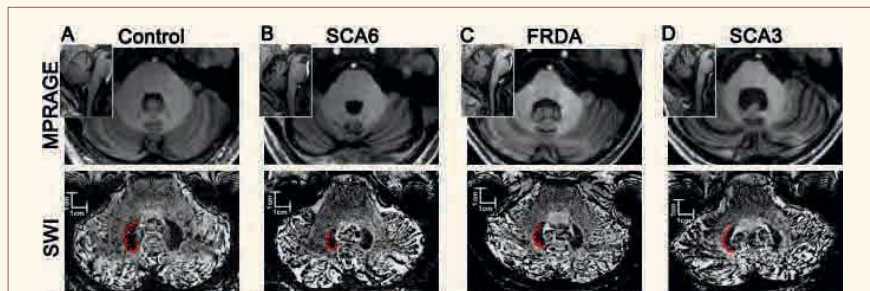


Fig. 11: Characteristic structural 7T MRI examples of (A) a control subject, (B) a SCA6 patient, (C) a FRDA patient, and (D) a SCA3 patient. Top row shows axial slices of MPRAGE acquisition. Small insert shows sagittal images. Marked cerebellar atrophy is seen in the SCA6 patient, large fourth ventricle in the SCA3 patient, and mild atrophy of the spinal cord in the FRDA patient. Second row shows axial slices of SWI acquisition of the same subjects. Dentate nuclei are seen as hypointensities. Drawings of the dentate nuclei are superimposed on the left (red). Dentate nuclei were smaller in the three patients. Dentate atrophy was most marked in the SCA6 patient. (Figure taken from [7])

Dagmar Timmann, Maria R. Stefanescu, Andreas Deistung
Jürgen Reichenbach, Mark E. Ladd

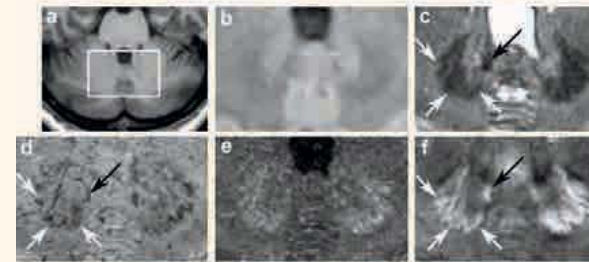


Fig. 12: MRI of the cerebellar nuclei at 3T. T1-weighted image, FLAIR image, T2-weighted image, susceptibility weighted image, effective transverse relaxation ($R2^*$) map, and quantitative susceptibility map are shown from (a) to (f), respectively. The white box in (a) marks the region of the enlarged sections shown in (b-f). The white and black arrows indicate the dentate nucleus and the emboliform nucleus, respectively.

The depiction of the cerebellar nuclei on QSM is superior to the other contrasts due to its high signal-to-noise ratio and the high local contrast of the cerebellar nuclei (Figure taken from [3])

nuclei is artificially increased in SWI phase images, and cerebellar nuclei volumes assessed on the SWI images do not reflect the actual volumes. These limitations are largely overcome by its offspring, the so-called quantitative magnetic susceptibility mapping (QSM) technique. Work by Andreas Deistung and Jürgen Reichenbach has shown that QSM is not only able to assess the local magnetic susceptibility distribution in brain tissue in vivo but also to provide substantially improved anatomical delineation of deep gray matter structures including the deep cerebellar nuclei (Fig. 12; [1,2]). Being a quantitative method, QSM enables quantification of changes in iron content, allowing monitoring of possible disease-related changes in iron deposition.

In 2015 the German Research Foundation (DFG) granted funding of a collaborative project between the University Clinic Essen, the Erwin L. Hahn Institute for Magnetic Resonance Imaging and the Jena University Hospital. The aim of the collaborative project is to apply novel MRI approaches including QSM to obtain deeper insight into the pathoanatomy of cerebellar nuclei and to utilize it clinically in common forms of degenerative ataxias. Structural MRI of the cerebellar nuclei will be extended to other hereditary ataxias, that is sporadic ataxias, multiple system atrophy (cerebellar type, MSA-C), and spinocerebellar ataxias types 1, 2, and 17 (SCA1, SCA2, SCA17). Furthermore, long-term studies will be performed to determine whether quantification of nuclear pathology is a useful biomarker of disease progression and response to therapeutic interventions. Because MRI at 7T is superior to that at 3T

considering signal-to-noise ratio, contrast, and spatial resolution, the diagnostic benefit of MRI imaging will be compared at 7T vs. 3T.


References

- [1] Deistung A, Schäfer A, Schweser F, Biedermann U, Güllmar D, Trampel R, Turner R, Reichenbach JR (2013). High-resolution MR imaging of the human brainstem in vivo at 7 Tesla. *Frontiers in Human Neuroscience* 7, 710.
- [2] Deistung A, Schäfer A, Schweser F, Biedermann U, Turner R, Reichenbach JR (2013). Toward in vivo histology: a comparison of quantitative susceptibility mapping (QSM) with magnitude-, phase-, and $R2^*$ -imaging at ultra-high magnetic field strength. *Neuroimage* 65, 299-314.
- [3] Deistung A, Stefanescu MR, Ernst TM, Schlamann M, Ladd ME, Reichenbach JR, Timmann D (2015). Structural and functional magnetic resonance imaging of the cerebellum: Considerations for assessing cerebellar ataxias. *Cerebellum* [Epub ahead of print]
- [4] Diedrichsen J, Maderwald S, Küper M, Thürling M, Rabe K, Gizewski ER, Ladd ME, Timmann D (2011). Imaging the deep cerebellar nuclei: a probabilistic atlas and normalization procedure. *Neuroimage* 54, 1786-94.
- [5] Maderwald S, Thürling M, Küper M, Theysohn N, Müller O, Beck A, Aurich V, Ladd ME, Timmann D (2012). Direct visualization of cerebellar nuclei in patients with focal cerebellar lesions and its application for lesion-symptom mapping. *Neuroimage* 63:1421-31.
- [6] Solbach K, Kraff O, Minnerop M, Beck A, Schöls L, Gizewski ER, Ladd ME, Timmann D (2014). Cerebellar pathology in Friedreich's ataxia: atrophied dentate nuclei with normal iron content. *Neuroimage Clin* 6:93-9.
- [7] Stefanescu MR, Dohnalek M, Maderwald S, Thürling M, Minnerop M, Beck A, Schlamann M, Diedrichsen J, Ladd ME, Timmann D (2015). Structural and functional MRI abnormalities of cerebellar cortex and nuclei in SCA3, SCA6 and Friedreich's ataxia. *Brain* 138:1182-97.

Research groups at the ELH

Prof. Dr. Harald Quick
(University Hospital Essen)

- Development of high field MR methodology and hardware
- Clinical application development for 7T high-resolution MRI in oncologic and cardiovascular body imaging
- Simulation and development of 7T RF coils
- B1-shimming concepts for 7T body MRI
- High field MR safety and implants



Structural elements of 7T-body MRI system, receive body RF coil and transmit for 7T high-resolution MRI of the small bowel (T1 and T2 contrast)

Prof. Dr. Matthias Brand
(University Duisburg-Essen)

- Neural correlates of higher cognitive and emotional brain functions:
 - decision making
 - human-robot interaction
 - craving reactions on addiction-related stimuli
- Contribution to functional/anatomical segregation of the prefrontal cortex and limbic regions which cannot be done efficiently with lower field strengths




Ventral striatum activity in cocaine addiction (Brand et al., NeuroImage 2010)




Decision making and food labels: impact of amygdala activity (Schneiders et al., 2013, NeuroImage)

Assoc. Prof. Dr. Tom Scheenen
(Radboud University Medical Center Nijmegen)


- Multi-parametric MR of prostate cancer
- ¹H and ³¹P spectroscopic imaging of the prostate
- ¹H and ¹³C spectroscopic imaging of the brain
- USPIO-enhanced detection of metastatic lymph nodes in cancer
- Related RF coil development



T2-weighted MRI and diffusion-weighted MRI of the prostate



B1-shimmed, NOE enhanced ¹³C-MRSI of the brain




¹³C-MRSI of prostate cancer (arrows): increased GPC signal

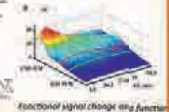


Prof. Dr. David Norris
(Donders Institute Nijmegen)

- High spatial resolution functional MRI
- GABA spectroscopy in the brain
- Methods for fMRI data acquisition
- Simultaneous multi-slice imaging techniques
- High resolution anatomical imaging of the brain




GABA spectra recorded at three different locations in the brain at 7T



Functional signal change (in functional echo time (fE)) and cortical depth for human visual cortex at 7T

Prof. Dr. Mark Ladd
(German Cancer Research Center Heidelberg)


- Whole-body imaging at 7T including RF manipulation strategies using parallel transmission
- Numerical simulation and implant safety
- Development of a 32-channel parallel transmission system
- Quality assurance standards for ultra-high-field imaging




Axial and coronal systems acquired in the abdomen (left) with B1-shimmed RF array placed on the bore floor of the 7T system (right)

Prof. Dr. Dagmar Timmann
(University Hospital Essen)

- Physiology and pathophysiology of the human cerebellum
- High-resolution structural MRI of the cerebellar nuclei in health and disease (ataxias)
- Functional MRI of the deep cerebellar nuclei
- Involvement of the cerebellum in motor learning
- Rehabilitation of cerebellar ataxias



Structural MRI of the cerebellar nuclei in ataxias (Schneiders, Ladd & Timmann, Brain 2012)



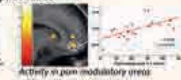
Functional MRI of the cerebellar nuclei (Schneiders, Ladd & Timmann, Journal of Neurophysiology 2012)

Prof. Dr. Ulrike Bingel
(University Hospital Essen)

- Pain processing and modulation in health and disease
 - Mechanisms of placebo and nocebo responses
 - Cognition and pharmacotherapy
 - Impact of pain on cognitive processes



fMRI pain processing areas (Wager et al., NeuroImage 2005)



Activity in pain modulatory system with positive expectancy



Behavioural fMRI

Pain-specific modulation of hippocampal activity and functional connectivity during visual encoding (Schneiders et al., Journal of Neurophysiology 2012)



Understanding the neural circuitry of pain processing and pain modulation

Ulrike Bingel

Chronic pain conditions affect up to 15% of the adult population and represent a major burden to the individuals and society. The underlying mechanisms of an individual's pain sensitivity, susceptibility for pain chronification and ability to modulate pain under distinct contextual circumstances are incompletely understood. Ulrike Bingel's group investigates these mechanisms using functional and structural brain imaging in combination with pharmacological and psychophysical approaches in healthy volunteers and in patient groups suffering from chronic pain or neurological disorders frequently associated with pain, such as Parkinson's Disease. As part of this research focus her group also investigates the detrimental effects of acute and chronic pain on cognitive processes which represents a major complaint in patients suffering from pain. Another strand of research is dedicated to study the neurobiological mechanisms of placebo- and nocebo responses and their contribution to active medical treatments. Recently, her group has moved on to study the contribution placebo mechanisms (expectation and associative learning) to the efficacy and tolerability of active pharmacological treatments. Together with Prof. Irene Tracey (FMRIB Centre, Oxford) she revealed that expectation crucially modulates analgesia in response to the potent opioid remifentanyl and that this interaction of drug action and cognitive factors is evident both at the behavioural and neurobiological level [1].

Neuroimaging at the ELH with ultra-high field strength provides the unique opportunity to focus on high resolution imaging of the brainstem and ideally the spinal cord, to further elucidate the contribution of distinct subcortical circuitry and the spinal cord to pain and pain modulation in health and disease. The collaboration with David Norris and Dagmar Timmann at the ELH represents an ideal situation to push forward these necessary methodological techniques.

References

- [1] U. Bingel, V. Wanigasekera, K. Wiech, R. Ni Mhuircheartaigh, M. C. Lee, M. Ploner, I. Tracey (2011). The effect of treatment expectation on drug efficacy: imaging the analgesic benefit of the opioid remifentanyl. *Sci Transl Med* 3, 70ra14; published online Epub Feb 16.

Sensorimotor interaction of nociceptive stimuli

Ulrike Bingel
Christoph Ritter

Pain is commonly defined as an unpleasant sensory and emotional experience associated with actual or potential tissue damage [1]. Pain is, thus, mostly conceptualized as a perceptual phenomenon. However, the crucial protective function of pain depends on appropriate motor and autonomic responses rather than on the perception of pain. Moreover, motor and autonomic processes are known to play an important role in the pathology and therapy of chronic pain. Chronic pain and motor behavior influence each other and the modulation of motor behavior (and motor processing in the brain) can be therapeutically beneficial. Similarly, autonomic dysfunctions have been implicated in the pathology of different chronic pain states. Consequently, motor and autonomic components of pain were conceptualized early as essential aspects of pain. However, how the brain translates noxious stimuli into motor and autonomic responses is far less well studied and understood than its perceptual aspects.

In the current project, we aim at characterizing the neural basis of sensorimotor integration in response to painful stimulation and the somatotopic outline of brain areas known to be involved in this integration process, such as the rostral cingulate zone, the supplementary motor area, the putamen and the primary sensorimotor cortex. To this end, we conceived several experiments with increasing complexity. The first functional magnetic resonance imaging study deals with the somatotopic representation of nociceptive information in our motor regions of interest. Using a rather simple paradigm, we applied painful or non-painful electrical shocks to either the dorsum of the left hand or the left foot and asked our volunteers to rate the intensity of the perceived stimulus on a visual analogue scale. We hypothesize that both functional connectivity between and activity within our sensory and motor target regions change in a somatotopic fashion. Future studies will also incorporate controlled motor tasks.

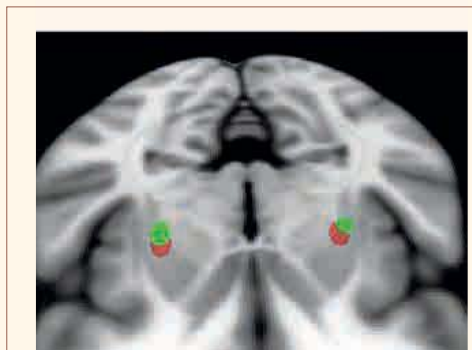


Fig. 13: Somatotopic representation of nociceptive information in the putamen

Means and standard error of the mean (SEM) of peak coordinates of differential contrasts painful vs. nonpainful stimulation of hand (red) and foot (green) in the putamen from 21 subjects projected onto the MNI template of the Harvard Oxford atlas (center of sphere: mean coordinate; extent of sphere in x, y and z direction: standard error of the mean).

References

- [1] H. Merskey, N. Bogduk (1994). *Classification of Chronic Pain*, 2nd ed., IASP Press, Seattle.

Clinical Imaging Applications at 7 Tesla

Research activities of our one-year clinical IFORES stipendiaries

In 2015 four clinical researchers received 12-months of intramural funding of the Medical Faculty, University of Duisburg-Essen (Interne Forschungsförderung Essen, IFORES), to conduct defined clinical research projects using 7T MRI at the Erwin L. Hahn Institute. The following medical doctors and project applications have received a 12-months IFORES stipend in 2015:

- Cornelius Deuschl, MD, Dept. of Radiology: 7T Therapy monitoring in brain tumors
- Britta Hüning, MD, Clinic for Pediatrics: Imaging of the cerebellum of adult very preterm infants at 7T
- Juliane Göbel, MD, Dept. of Radiology: 7T Cardiovascular MRI – Late gadolinium enhancement
- Andrea Lazik-Palm, MD, Dept. of Radiology: 7T MRI of hip cartilage

All IFORES projects reflect efforts and advances to assess and employ the inherent high signal-to-noise ratio (SNR) and the excellent soft-tissue contrast of 7-Tesla MRI to improve spatial resolution and image contrast in selected clinical MR imaging applications. Key motivation in this context is to explore potentially relevant clinical applications in high-field neuro and body MRI.

To achieve these goals, most of the current IFORES projects make use of the ELH-unique radiofrequency (RF) hardware and B1-shimming infrastructure at the ELH consisting of an 8-channel RF transmit/receive system, the capability for signal homogenization with the TIAMO (time interleaved acquisition of modes) method [1,2], and various custom-build multi-channel transmit/receive RF coils [3-5].

The clinical projects start off with feasibility testing and sequence parameter optimization in volunteers, followed by defined studies in patients. Here, 7T MRI with its potential advantages and, otherwise, challenges and limitations is compared in intra-individual comparisons to the respective clinical standard MR method at 1.5T and/or at 3T magnetic field strength.

The following short descriptions of the year 2015 IFORES projects may provide a brief insight into current and ongoing research with a clinical focus in 7T high field neuro and body MRI.

Cornelius Deuschl: Therapy monitoring with 7T MRI in high-grade glioma

Project summary

The aim of this study is to compare the diagnostic ability of 3T and 7T MRI for monitoring antiangiogenic treatment with Bevacizumab in patients with recurrent high-grade glioma. Three subjects with recurrent high grade glioma were enrolled up to now in this study. The study protocol for both field strengths comprised T1, SWI, FLAIR, ceMPRAGE and T2-weighted imaging. As results both, 3T and 7T MRI, could identify antiangiogenic effects of Bevacizumab. 7T provides a better visualization of microvasculature changes and helps to identify the reduction of peritumoral neovascularization in more detail (Fig. 14). 7T MRI might contribute to differentiate responders from non-responders and improve therapy.

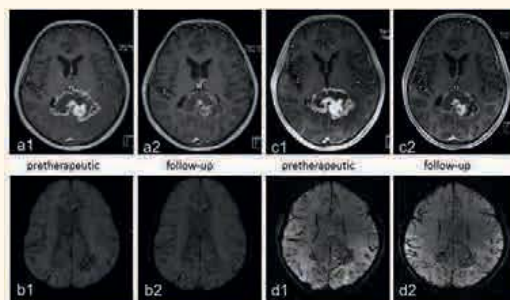


Fig. 14: Recurrent high-grade glioma show at baseline central necrosis and periphery, irregular contrast enhancement with nodular components (3T: a1, 7T: c1). After three cycles of Bevacizumab contrast enhancement decreases, which can be better seen at 7T (3T: a2, 7T: c2). Microvasculature changes can be detected on susceptibility weighted imaging (3T: b1, 7T: d1), whereas higher field strengths provides improved visualization. After Bevacizumab-therapy a decreased number of peritumoral vessels can be detected, which can be better seen on 7T compared to 3T (3T: b2, 7T: d2).

Harald H. Quick, Cornelius Deuschl
Britta Hüning, Juliane Göbel, Andrea Lazik-Palm

Britta Hüning: 7T MRI of the cerebellum of adult very preterm infants

Project summary

In adulthood cerebellar lesions are predominantly associated with motor deficits, whereas during childhood cognitive impairment and behaviour problems are more common. There is increasing evidence that cerebellar development may be impeded in very preterm infants and contribute to cognitive dysfunction later in life. As yet most studies examined the volume of the cerebellum which has been shown to be reduced in adults who have been very preterm infants. Little is known about possible changes of the main output structure of the cerebellum that is the deep cerebellar nuclei. In the present study, in addition to volumetric measures of the cerebellar cortex and its subdivisions, susceptibility-weighted imaging

(SWI) is used to visualize the cerebellar nuclei (in particular the largest one, that is the dentate nucleus) and calculate their volume. SWI is performed in adult very preterm infants both at a magnetic field strength of 3T and the ultrahigh magnetic field strength of 7T. Because of increasing susceptibility effects with increasing field strength, more detailed visualization and quantification of possible abnormalities of the dentate nuclei are expected at 7T (Fig. 15). Imaging data will be correlated with behavioural measures including cognitive function and classical eyeblink conditioning. This simple motor learning paradigm is known to critically depend on the integrity of the cerebellum. Imaging studies are performed under supervision of Harald Quick's group, behavioural data are collected and analysed in collaboration with Dagmar Timmann's group.

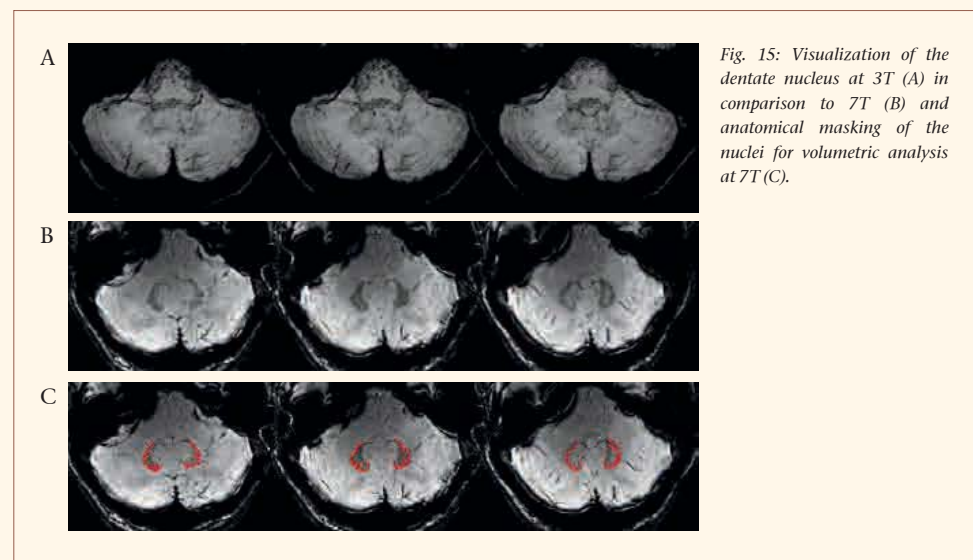


Fig. 15: Visualization of the dentate nucleus at 3T (A) in comparison to 7T (B) and anatomical masking of the nuclei for volumetric analysis at 7T (C).

Juliane Göbel: 7T Cardiovascular MRI – Late gadolinium enhancement
Project summary

Late gadolinium enhancement (LGE) plays a major role in cardiac MR imaging because it allows for the detection of myocardial fibrosis/scarring. At 1.5T LGE imaging is limited due to a relatively low spatial resolution and a limited signal-to-noise-ratio. These restrictions might be overcome by MR imaging at 7T - although numerous technical challenges exist at 7T that render cardiovascular MRI at this field strength difficult. Thus, with the clinical motivation to improve LGE MRI at high field strength, this study aimed towards identifying and resolving the remaining technical hurdles that need to be overcome to assess the full potential of 7T MRI.

Initially, an adiabatic Wideband Uniform Rate Smooth Truncation (WURST) pulse was implemented in an Inversion Recovery Fast Low Angle Shot sequence (IR-FLASH) in order to homogeneously invert the longitudinal magnetization at 7T. This WURST-IR-FLASH sequence was then tested for safety and for homogeneous image appearance in 7 healthy volunteers. Subsequently, three patients without any contraindication for MRI at 7T and with known myocardial scarring were scanned at 3T and at 7T including LGE imaging. An 8-channel body transmit/receive radiofrequency (RF) coil was employed. Cardiac triggering was performed using the pulse triggering unit of the MRI system. Preliminary results are that in none of the three patients LGE images with a diagnostic image quality could be achieved (Fig. 16) yet. The inversion of the magnetization appeared to be incomplete, resulting in an inhomogeneous greyish appearance of the myocardium. This is most likely due to insufficient RF energy transmission by the employed WURST pulse for complete 180° inversion of the longitudinal magnetization. Accordingly, the next step in this project is the adaption of the RF power and WURST pulse to optimize the excitation flip angle.

Andrea Lazik-Palm: New horizons of 7T MRI in musculoskeletal applications
Project summary

After a comprehensive 7 Tesla hip cartilage protocol was established in 2014 [6,7], the research focus in 2015 was set on the application of this protocol in patients and the comparison of 7 Tesla image quality to lower magnetic field strengths. The protocol not only included high resolution DESS, T1 and PDw sequences for morphological imaging, but also T1-mapping after intravenous contrast agent administration (delayed gadolinium enhanced MRI of cartilage, “dGEMRIC”), T2- and T2*-mapping for evaluation of cartilage composition. This protocol proved high image quality in a previous volunteer study [8]. The patients, who had been treated with autologous cartilage transplantation due to a focal cartilage defect, all tolerated the 7 Tesla MRI examination well and also participated in a comparable 3 Tesla scan. The results at 7T predominantly showed superiority regarding image quality, assessment of cartilage pathologies, and contrast over 3T MRI (Fig. 17) and therefore pave the way to a clinical reasonable application of ultra-high field musculoskeletal MRI.

Not only the hip, but also the shoulder joint was in the focus of our research in 2015. After the construction of 7-channel local receive RF coil, added to the in-house developed 8-channel transmit/receive shoulder RF coil, we were able to establish a comprehensive 7 Tesla shoulder protocol with a focus on turbo-spin echo sequences, which are on the one hand the most favorable techniques in shoulder MRI, but on the other hand the most difficult sequences to be implemented in an ultra-high field setting. In an ongoing study, we evaluate the validity of 7 Tesla MRI in patients suffering from rotator cuff tears in comparison to the surgical report (Fig 18).

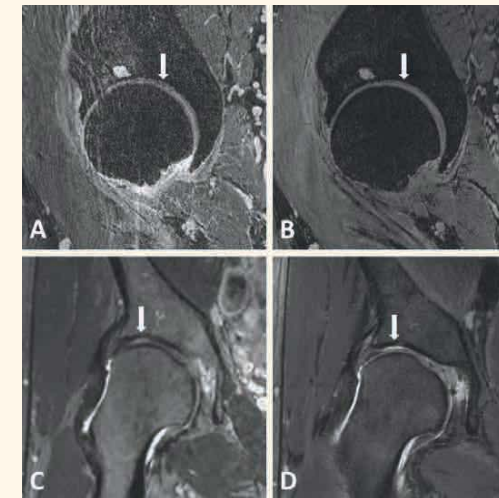


Fig. 17: Sagittal images of a patient after autologous cartilage transplantation in the hip at 3 Tesla (A, C) and 7 Tesla (B, D). In the T1w VIBE sequence (A, B) with comparable parameters at 3T and 7T, better image quality at 7T is obvious with less noise and better delineation of acetabular and femoral cartilage layers (arrow). Also in PDw imaging (C, D) 7T proves superiority regarding delineation and contrast of the cartilage transplant (arrow).

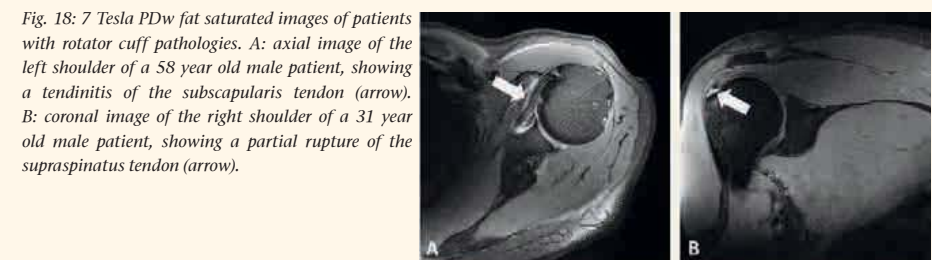
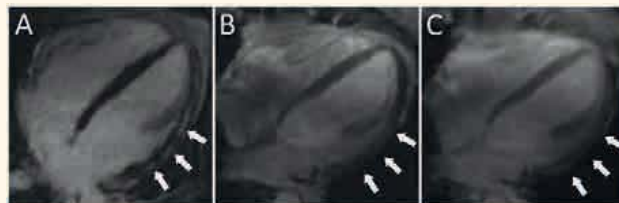


Fig. 18: 7 Tesla PDw fat saturated images of patients with rotator cuff pathologies. A: axial image of the left shoulder of a 58 year old male patient, showing a tendinitis of the subscapularis tendon (arrow). B: coronal image of the right shoulder of a 31 year old male patient, showing a partial rupture of the supraspinatus tendon (arrow).

Fig. 16: Late gadolinium enhancement (LGE) imaging in a 32-year-old male with state after myocarditis. A: T1-weighted IR-FLASH sequence, 10 min after contrast agent injection, individually adjusted TI, 3T) showing an obvious streak of subepicardial LGE in the lateral wall of the left ventricle (arrows). B and C: Adiabatic WURST-IR-FLASH at 7T (B: TI=200 ms, C: TI=350 ms) showing an insufficient inversion with an inhomogeneous greyish appearance of the myocardium (arrows).



References

- [1] Orzada S, Maderwald S, Poser BA, Bitz AK, Quick HH, Ladd ME. RF excitation using time interleaved acquisition of modes (TIAMO) to address B1 inhomogeneity in high-field MRI. *Magn Reson Med.* 2010; 64:327-333.
- [2] Orzada S, Maderwald S, Poser BA, Johst S, Kammergesser S, Ladd ME, Bitz AK. Time-interleaved acquisition of modes: an analysis of SAR and image contrast implications. *Magn Reson Med.* 2012; 67:1033-1041.
- [3] Kraff O, Bitz AK, Dammann P, Ladd SC, Ladd ME, Quick HH. An eight-channel transmit/receive multipurpose coil for musculoskeletal MR imaging at 7 T. *Med Phys.* 2010; 37:6368-6376.
- [4] Kraff O, Bitz AK, Kruszona S, Orzada S, Schaefer LC, Theysohn JM, Maderwald S, Ladd ME, Quick HH. An eight-channel phased array RF coil for spine MR imaging at 7 T. *Invest Radiol.* 2009; 44:734-740.
- [5] Rietsch SH, Quick HH, Orzada S. Impact of different meander sizes on the RF transmit performance and coupling of microstrip line elements at 7 T. *Med Phys.* 2015 Aug;42(8):4542-52.
- [6] Theysohn JM, Kraff O, Orzada S, Theysohn N, Classen T, Landgraeber S, Ladd ME, Lauenstein TC. Bilateral hip imaging at 7 Tesla using a multi-channel transmit technology: initial results presenting anatomical detail in healthy volunteers and pathological changes in patients with avascular necrosis of the femoral head. *Skeletal Radiol.* 2013; 42:1555-1563.
- [7] Theysohn JM, Kraff O, Theysohn N, Orzada S, Landgraeber S, Ladd ME, Lauenstein TC. Hip imaging of avascular necrosis at 7 Tesla compared with 3 Tesla. *Skeletal Radiol.* 2014; 43:623-632.
- [8] Lazik A, Theysohn JM, Geis C, Johst S, Ladd ME, Quick HH, Kraff O. 7 Tesla quantitative hip MRI: T1, T2 and T2* mapping of hip cartilage in healthy volunteers. *Eur Radiol.* 2015 Aug 28. [Epub ahead of print]

Coming soon: The new ELH Homepage

The Internet presence of the ELH will appear in a new design soon, more clearly structured and containing new and updated contents. Here you get some first impressions. You will find the new homepage just like the old one via www.hahn-institute.de.



News



Cooperation

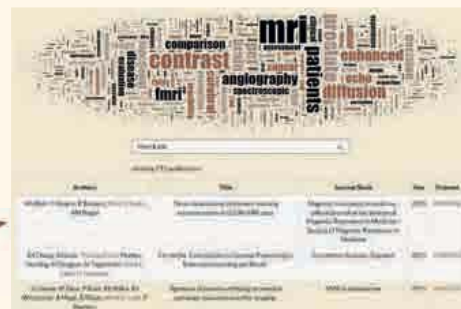


People



Research

Publications



Personell and Organisational Structure at ELH

Directorate / Principal Investigators

Managing Director / PI
 Prof. Dr. Harald H. Quick
Director / PI
 Prof. Dr. David Norris
 Prof. Dr. Matthias Brand

PI
 Prof. Dr. Ulrike Bingel
 Prof. Dr. Timmann-Braun
 Assoc. Prof. Dr. Tom Scheenen
 Prof. Dr. Mark E. Ladd

Management

Administrative Director
 Dr. Corinna Heldt
ELH-Physicists
 Dr. Oliver Kraff
 Dr. Stefan Maderwald
Radiographer
 Lena Schäfer
Assistance
 Sigrid Radermacher
 Verena Broszeit

Scientists

Dr. Lauren Bains	Dipl.-Ing. Yacine Nouredine
MSc. Sascha Brunheim	Dr. med. Britta Hüning
Dr. med. Cornelius Deuschl	MSc. Mark Oehmigen
Dipl.-Phys. Thomas Ernst	Dr. Stephan Orzada
Dr. med. Juliane Göbel	MSc. Stefan Rietsch
Dr. rer. nat. Marcel Gratz	Dipl.-Psych. Christoph Ritter
MSc. Donghyun Hong	MSc. Morteza Rohani
Dr. Sören Johst	Prof. Dr. med. Indira Tendolkar
MSc. Irati Markuerkiaga	MSc. Jan-Willem Thielen
Priv.-Doz. Dr. med. Christoph Mönninghoff	Dipl.-Psych. Patrick Trotzke
	Dipl.-Ing. Maximilian Völker

Students

Eileen Frerk
 Luisa Bräuer
 BSc. Anna Brol
 Sarah Handtke
 BSc. Viktor Pfaffenrot

New in 2015

Ical Boztepe
 Luisa Bräuer
 Anna Brol
 Verena Broszeit
 Sascha Brunheim
 Cornelius Deuschl
 Rossitza Draganova
 Sarah Handtke
 Corinna Heldt
 Björn Koch
 Irati Markuerkiaga
 Ivan Maximov
 Danisha Perenpamoorthy
 Viktor Pfaffenrot
 Daniel Sharoh

Left in 2015

Rasim Boyacioglu
 Ical Boztepe
 Bixia Chen
 Niravkumar Darji
 Martina Flöser
 Christian Kärger
 Maria Hahnemann
 Katharina Hauprich
 Andrea Lazik-Palm
 Matthias Meyer
 Danisha Perenpamoorthy
 Michael Schwarz
 Eileen Frerk
 Juliane Göbel
 Johannes Grüneisen
 Bart van de Bank



Current Grants

Scheenen, T. W., Quick, H. H., Barentsz, J. O.; Nanotechnology at ultra-high magnetic field: towards in vivo detection of small lymph node metastases with MRI Radboudumc (2016-2020)

Brand, M.; User centred social media – decision support in social media German Research Foundation (2015-2019)
Timmann, D., Ladd, M. E., Deistung, A., Reichenbach, J.; In vivo assessment of the cerebellum by novel MRI techniques and application to hereditary ataxias: morphological, pathoanatomical and clinical aspects German Research Foundation (2015-2018)

Brand, M.; Neural correlates of craving in patients with pathological buying – an fMRI study with a cue-reactivity paradigm German Research Foundation (2015-2017)

Rennings, A., Solbach, K., Quick, H. H.; Untersuchung von Electronic Band Gap (EBG) HF-Spulen für die 7T MRT German Research Foundation (2015-2016)

Norris, D. G.; Language regions in Interaction: An investigation of directional connectivity in the human language system using laminar fMRI Netherlands Organisation for Scientific Research (2014-2018)

Philips, B., Scheenen, T. W.; Multi-parametric MRI of the prostate cancer: the next level Dutch Cancer Society (2014-2017)

Timmann, D., Ladd, M. E.; Contribution of the human cerebellum to extinction learning and renewal, Project in the Research Unit FOR 1581 “Extinction Learning: Neural Mechanisms, Behavioural Manifestations, and Clinical Implications” German Research Foundation (2014-2016)

Quick, H. H.; IFORES: Internal stipends for clinical researchers from University Hospital Essen Medical Faculty, University of Duisburg-Essen (2014-2015)

Ladd, M. E., Speck, O., Norris, D. G.; German ultrahigh field imaging (GUFi), Core Facility German Research Foundation (2013-2016)

Ladd, M. E.; MRexcite: Unlocking the potential of ultra-high-field MRI through manipulation of radiofrequency excitation fields in human tissue European Research Council Advanced Grant (2012-2017)

Tschöp, M., Norris, D. G., Tendolkar, I., Wiltfang, J.; Imaging and Curing Environmental Metabolic Diseases (ICEMED) Helmholtz Gemeinschaft (2012-2017)

Gowland, P., Ladd, M. E., Norris, D. G., Möller, H. E., Speck, O., Jezzard, P., Del Guerra, A., Hoogduin, J. M., Stancanello, J., De Boer, R., Roell, S., Lanz, T., Oberle, M., Stacey, N.; HiMR: Ultra-high field magnetic resonance imaging EU FP7 Marie Curie Initial Training Networks (ITN) (2012-2016)

Scheenen, T. W.; EXACTA: Exploring the aggressiveness of prostate cancer to enable an individualised treatment approach European Research Council Starting Grant (2010 -2015)

Awards

Prof. Dr. Harald H. Quick, Magnetic Resonance Imaging Award 2015, awarded at the 16th international MRI Symposium „MR 2015“ in Garmisch, award for outstanding scientific work in particular for ultra high-field magnetic resonance and hybrid PET/MR-imaging.

Prof. Dr. Dagmar Timmann-Braun and Prof. Dr. Friedhelm Hummel, Felgenhauer-Symposium 2015 „The cerebellum and its role during learning and neurological diseases“, Stiftung Felgenhauer and Deutsche Gesellschaft für Neurologie.

Prof. Dr. Dagmar Timmann-Braun, Fellow 2015: Society for the Research on the Cerebellum.

Dr. Katarina Forkmann, EFIC-Grünenthal Grant 2015.

Dr. Sören Johst, Erwin L. Hahn Institute Award for Young Scientists 2015 for his thesis “Acquisition Methods for 7 Tesla MRI from Head to Toe”.

Nicolai Spicher, Bsc. Award of the „Deutsche Gesellschaft für Medizinische Informatik, Biometrie und Epidemiologie“, 60th GMDS Jahrestagung 2015 in Krefeld for his graduation work „Ultra High-Field MRI: Implementation and Evaluation of the Eulerian Video Magnification for peripheral pulse triggering“.

Dr. Gregor und Dr. Yasmin Eschrat Zaun, thesis award 2015 of the Medical Faculty of the University Duisburg-Essen: Dr. Gregor Zaun „Effekte starker statischer Magnetfelder auf die Spermatogenese und männliche Fertilität im Mausmodell“ and Dr. Yasmin Eschrat Zaun „Auswirkungen starker statischer Magnetfelder auf die weibliche Reproduktion und die Fertilität im Mausmodell“.



Dr. Sören Johst, winner of the Erwin L. Hahn prize 2015 with the team of directors and Prof. Siegfried Trattnig, keynote speaker at the Erwin L. Hahn Lecture 2015.

Participation at ISMRM 2015 in Toronto

- Andreas Bitz:** Maxwell equations & EM field modeling for MRI; Session: MR Physics for Physicists; educational talk
- Andreas Bitz:** Weekend Educational Course: RF Engineering - Coils; moderator
- Bixia Chen:** Giant intracranial aneurysms at 7 Tesla MRI: A new diagnostic approach to understand this rare intracranial vascular pathology; Session: High Field Applications; power pitch (oral presentation and e-poster)
- Bixia Chen:** Effect of cranial fixation plates on brain MR imaging at 7T in neurosurgical patients; Session: Safety in MRI; e-poster
- Thomas Fiedler:** RF safety assessment of a bilateral 4-channel Tx/Rx 7T breast coil; Session: Safety in MRI; e-poster
- Thomas Fiedler:** Local SAR elevations in the human head induced by high-permittivity pads at 7 Tesla; Session: Safety in MRI; e-poster
- Martina Flöser:** Comparison of local and remote transmit arrays for body imaging at 7T under power and local SAR constraints; Session: Parallel Transmission Strategies; talk
- Martina Flöser:** Hybrids of static and dynamic RF shimming for body imaging at 7T; Session: RF Pulse Design; e-poster
- Marcel Gratz:** Semi-automatic quantification of long-term stability and image quality of a parallel transmit system at 7T; Session: Image Quality Assessment; traditional poster
- Maria Hahnemann:** Comparison of T2-Weighted MRI of the Small Bowel at 7 Tesla and 1.5 Tesla; Session: Diabetes, Metabolism & GI; talk
- Maria Hahnemann:** Contrast-Enhanced T1-Weighted MRI of the Small Bowel at 7 Tesla in Comparison to 1.5 Tesla; Session: Diabetes, Metabolism & GI; talk
- Sören Johst:** An 8-channel parallel transmit system for 7T MRI based on custom-built I/Q modulators; Session: UHF Acquisitions: Neuro; e-poster
- Oliver Kraff:** MR safety of implants: how to separate the good from the bad & the ugly; Session: A Practical Guide to MRI Safety; educational talk
- Oliver Kraff:** In vivo comparison of B1 mapping techniques for hip joint imaging at 7 Tesla; Session: B1 Imaging; traditional poster
- Mark Ladd:** Transmit Arrays & Circuitry; Session: RF Engineering: Coils; educational talk
- Mark Ladd:** Weekend Educational Course: A Practical Guide to MR Safety; organizer/moderator
- Mark Ladd:** High Field Systems & Applications Study Group; Vice-Chair
- Miriam Lagemaat:** To NOE or Not to NOE? - a study about the use of the Nuclear Overhauser Effect in 31P MRSI of the brain at 7T; Session: MRS Data Processing Quantitation of MRSI Acquisition Method; e-poster
- Andrea Lazik:** A comprehensive 7 Tesla MRI protocol for quantitative (T1-, T2-, T2*-mapping) and morphological hip cartilage imaging; Session: Cartilage Imaging - Technical Developments; e-poster
- Yacine Noureddine:** RF-Induced Heating in MRI of Tissue Around an Aneurysm Clip Near the Middle Cerebral Artery at 7 T Under Consideration of the Pennes Bioheat Equation; Session: Safety in MRI; e-poster
- Stephan Orzada:** An integrated 8-channel Tx/Rx body coil for 7 Tesla whole-body MRI; Session: RF Coil Arrays; Talk
- Stephan Orzada:** A receive chain add-on for implementation of a 32-channel integrated Tx/Rx body coil and use of local receive arrays at 7 Tesla; Session: RF Coil Arrays; e-poster
- Bart Philips:** MRS data processing quantitation of MRSI acquisition method; Session: MRS Data Processing Quantitation of MRSI Acquisition Method; e-poster
- Harald Quick:** Technical Foundations: CE-MRA, Acceleration Methods; Session: Cardiovascular MRI: Vascular Flow & Angiography; educational talk
- Stefan Rietsch:** Impact of different meander sizes on the RF transmit performance and decoupling of micro strip line elements at 7T; Session: RF Engineering; traditional poster
- Samaneh Shoostary:** Stability test method for cartesian feedback power amplifier in pTx array; Session: UHF Applications: General; e-poster
- Tom Scheenen:** Applications of 7T in Cancer; Session: Clinical Cancer MRI: Case-Based; educational course
- Nicolai Spicher:** In Vivo 7T MR Imaging Triggered by Phase Information Obtained from Video Signals of the Human Skin; Session: Motion Correction Head; traditional poster
- Bart van de Bank:** Boosting 31P signals by using a 7 channel receive array at 7T; Session: RF Coil Arrays; e-poster
- Maximilian Völker:** The traveling heads: Initial comparisons of multicenter data on 7 Tesla MRI systems; Session: UHF Acquisitions: Neuro; e-poster

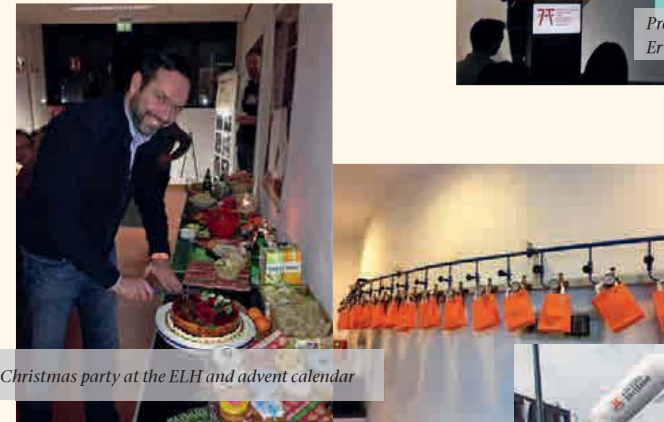
Erwin L. Hahn Moments 2015



Always a smiling face at the reception



Prof. Siegfried Trattnig, MD giving the Erwin L. Hahn Lecture



Christmas party at the ELH and advent calendar



Running event on Zollverein



Visit of the Commissioners of the king of the provinces of Gelderland and Overijssel, Clemens Cornielje and Ank Bijleveld and Franz-Josef Lersch-Mense, the NRW Minister for Federal Affairs, Europe and Media on November, 13th

Publications

Barth M., Breuer F., Koopmans P. J., Norris D. G., Poser B. A. (2015). Simultaneous multislice (SMS) imaging techniques. *Magn Reson Med*. doi: 10.1002/mrm.25897. [Epub ahead of print].

Boyacioglu R., Schulz J., Koopmans P. J., Barth M., Norris D. G. (2015). Improved sensitivity and specificity for resting state and task fMRI with multiband multi-echo EPI compared to multi-echo EPI at 7T. *Neuroimage*. 119:352-61. doi: 10.1016/j.neuroimage.2015.06.089. [Epub ahead of print]

Chang, D. I., Lissek, S., Ernst, T. M., Thürling, M., Uengoer, M., Tegenthoff, M., Ladd, M. E., & Timmann, D. (2015). Cerebellar Contribution to Context Processing in Extinction Learning and Recall. *Cerebellum*:14(6):670-6. doi: 10.1007/s12311-015-0670-z.

Deistung, A., Stefanescu, M.R., Ernst, T.M., Schlamann, M., Ladd, M.E., Reichenbach, J.R., Timmann, D. (2015). Structural and Functional Magnetic Resonance Imaging of the Cerebellum: Considerations for Assessing Cerebellar Ataxias. *Cerebellum* Oct 31. [Epub ahead of print]

Hahnemann, M.L., Kraff O., Maderwald S., Johst S., Orzada S., Umutlu L., Ladd M. E., Quick H.H., Lauenstein T. C. (2015). Non-enhanced magnetic resonance imaging of the small bowel at 7 Tesla in comparison to 1.5 Tesla: first steps towards clinical application. *Magn Reson Imaging*. doi: 10.1016/j.mri.2015.11.012. [Epub ahead of print]

Hahnemann, M. L., Kraff, O., Orzada, S., Umutlu, L., Kinner, S., Ladd, M. E., Quick, H. H., Lauenstein, T. C. (2015). T1-Weighted Contrast-Enhanced Magnetic Resonance Imaging of the Small Bowel: Comparison Between 1.5 and 7 T. *Invest Radiol.*: 50(8):539-47. doi: 10.1097/RLI.0000000000000161.

Holbach, M., Lambert, J., Johst, S., Ladd, M. E., & Suter, D. (2015). Optimized selective lactate excitation with a refocused multiple-quantum filter. *J Magn Reson*, 255, 34-38.

Johst, S., Maderwald, S., Fischer, A., Quick, H. H., Ladd, M. E., Orzada, S. (2015). Investigation of the saturation pulse artifact in non-enhanced MR angiography of the lower extremity arteries at 7 Tesla. *PLoS One*: 10(3):e0119845.

Kleinnijenhuis, M., van Mourik, T., Norris, D. G., Rüter, D. J., van Cappellen van Walsum, A. M., Barth, M. (2015). Diffusion tensor characteristics of gyrencephaly using high resolution diffusion MRI in vivo at 7T. *Neuroimage* 109:378-387.

Kraff, O., Fischer, A., Nagel, A.M., Mönninghoff, C., Ladd, M.E. (2015). MRI at 7 Tesla and above: demonstrated and potential capabilities. *Journal of magnetic resonance imaging: JMRI* 41:13-33.

Küper, M., Kaschani, P., Thürling, M., Stefanescu, M. R., Burciu, R. G., Göricke, S., Maderwald, S., Ladd, M. E., Hautzel, H., Timmann, D. (2015). Cerebellar fMRI Activation Increases with Increasing Working Memory Demands. *Cerebellum (London, England)*.

Lagemaat, M. W., Breukels, V., Vos, E. K., Kerr, A. B., van Uden, M. J., Orzada, S., Bitz, A. K., Maas, M. C., Scheenen, T. W. (2015). 1H MR Spectroscopic Imaging of the Prostate at 7T Using Spectral-Spatial Pulses. *Magn Reson Med*. doi: 10.1002/mrm.25569. [Epub ahead of print]

Lagemaat M. W., van de Bank B. L., Sati P., Li S., Maas M. C., Scheenen T. W. (2015). Repeatability of 31 P MRSI in the human brain at 7T with and without the nuclear Overhauser effect. *NMR Biomed*. doi: 10.1002/nbm.3455. [Epub ahead of print]

Lagemaat, M. W.; Maas, M. C.; Vos, E. K.; Bitz, A. K.; Orzada, S.; Weiland, E.; Van Uden, M. J.; Kobus, T.; Heerschap, A.; Scheenen, T. W. J. (2015). 31P MR spectroscopic imaging of the human prostate at 7 T: T1 relaxation times, Nuclear Overhauser Effect, and spectral characterization. *Magn Reson Med*: 73(3):909-20

Lazik, A., Theysohn, J. M., Geis, C., Johst, S., Ladd, M. E., Quick, H. H., Kraff, O. (2015). 7 Tesla quantitative hip MRI: T1, T2 and T2* mapping of hip cartilage in healthy volunteers. *European radiology*.

Matsushige, T., Chen, B., Dammann, P., Johst, S., Quick, H.H., Ladd, M.E., Forsting, M., Sure, U., Wrede, K.H. (2015). Microanatomy of the subcallosal artery: an in-vivo 7 T magnetic resonance angiography study. *Eur Radiol*. Nov 24. [Epub ahead of print]

Matsushige T., Chen B., Ringelstein A., Umutlu L., Forsting M., Quick H. H., Sure U., Wrede K. H. (2015). Giant Intracranial Aneurysms at 7T MRI. *AJNR Am J Neuroradiol*. [Epub ahead of print]

Moenninghoff, C., Kraff, O., Maderwald, S., Umutlu, L., Theysohn, J. M., Ringelstein, A., Wrede, K. H., Deuschl, C., Altmepfen, J., Ladd, M. E., Forsting, M., Quick, H. H., Schlamann, M. (2015). Diffuse axonal injury at ultra-high field MRI. *PLoS One*: 10(3):e0122329.

Noebauer-Huhmann, I.M., Szomolanyi, P., Kronnerwetter, C., Widhalm, G., Weber, M., Nemeč, S., Juras, V., Ladd, M.E., Prayer, D., Trattnig, S. (2015). Brain tumours at 7T MRI compared to 3T--contrast effect after half and full standard contrast agent dose: initial results. *European radiology* 25:106-112.

Noureddine, Y., Bitz, A. K., Ladd, M. E., Thürling, M., Ladd, S. C., Schaefer, G., Kraff, O. (2015). Experience with magnetic resonance imaging of human subjects with passive implants and tattoos at 7 T: a retrospective study. *Magma*: 28(6):577-90. doi: 10.1007/s10334-015-0499-y.

Rietsch, S. H. G., Quick, H. H., Orzada, S. (2015). Impact of different meander sizes on the RF transmit performance and coupling of microstrip line elements at 7 T. *Med Phys*: 42(8):4542

Scheenen, T., Rosenkrantz, A., Haider, M. & Fütterer, J. (2015). Multiparametric Magnetic Resonance Imaging in Prostate Cancer Management: Current Status and Future Perspectives. *Investigative radiology* 50(9):594-600.

Stefanescu, M. R., Dohnalek, M., Maderwald, S., Thürling, M., Minnerop, M., Beck, A., Schlamann, M., Diedrichsen, J., Ladd, M. E., & Timmann, D. (2015). Structural and functional MRI abnormalities of cerebellar cortex and nuclei in SCA3, SCA6 and Friedreich's ataxia. *Brain*, 138(Pt 5), 1182-97.

Thürling, M., Kahl, F., Maderwald, S., Stefanescu, R. M., Schlamann, M., Boele, H. J., De Zeeuw, C. I., Diedrichsen, J., Ladd, M. E., Koekkoek, S. K., & Timmann, D. (2015). Cerebellar cortex and cerebellar nuclei are concomitantly activated during eyeblink conditioning: a 7T fMRI study in humans. *J Neurosci*, 35(3), 1228-39.

van de Bank, B. L., Emir, U. E., Boer, V. O., van Asten, J. J., Maas, M. C., Wijnen, J. P., Kan, H. E., Oz, G., Klomp, D. W., Scheenen, T. W. (2015). Multi-center reproducibility of neurochemical profiles in the human brain at 7 T. *NMR Biomed*. 28(3):p.306-316.

van de Bank B. L., Orzada S., Smits F., Lagemaat M. W., Rodgers C. T., Bitz A. K., Scheenen T. W. (2015). Optimized (31) P MRS in the human brain at 7 T with a dedicated RF coil setup. *NMR Biomed*: 28(11):1570-8. doi: 10.1002/nbm.3422.

Wrede, K. H., Dammann, P., Johst, S., Mönninghoff, C., Schlamann, M., Maderwald, S., Sandalcioğlu, I. E., Ladd, M. E., Forsting, M., Sure, U., & Umutlu, L. (2015). Non-Enhanced MR Imaging of Cerebral Arteriovenous Malformations at 7 Tesla. *Eur Radiol*. [Epub ahead of print]





Photography
All images © Erwin L. Hahn Institute

Graphic design
AMP Studio, Duisburg



PARTICIPATING INSTITUTIONS



FAKULTÄT FÜR
INGENIEURWISSENSCHAFTEN



Radboud University Nijmegen



Radboudumc

Donders Institute
for Brain, Cognition and Behaviour

